International Journal of High Speed Electronics and Systems
Vol. 16, No. 1 (2006) 115–136
© World Scientific Publishing Company

Device Simulation Demands of Upcoming Microelectronics Devices

Hans Kosina and Siegfried Selberherr
Institute for Microelectronics, TU Vienna, Gusshausstrasse 27–29
A-1040 Vienna, Austria
{*Kosina*|*Selberherr*}*@iue.tuwien.ac.at*

Received 27 January 2005
Revised 29 June 2005
Accepted 30 June 2005

An overview of models for the simulation of current transport in micro- and nanoelectronic devices within the framework of TCAD applications is presented. Starting from macroscopic transport models, currently discussed enhancements are specifically addressed. This comprises the inclusion of higher-order moments into the transport models, the incorporation of quantum correction and tunneling models up to dedicated quantum-mechanical simulators, and mixed approaches which are able to account for both, quantum interference and scattering. Specific TCAD requirements are discussed from an engineer's perspective and an outlook on future research directions is given.

Keywords: Microelectronics, TCAD, device simulation, transport models, quantum effects.

1. Introduction

Integrated circuits play a key role in modern information society. The continuous increase in computing performance has been enabled by down scaling of integrated semiconductor devices. The minimum feature size of integrated circuits has been continuously reduced in the past decades, a trend that is expected to continue at an unaltered pace in the next decade, as predicted by the International Technology Roadmap for Semiconductors [1]. Today, the 90 nm CMOS technology with physical transistor gate lengths in the range of 40 nm is used in mass production. The functioning of MOS field effect transistors with 6 nm gate length has been demonstrated in research laboratories [2]. The success of microelectronics technology has partly been enabled by the aid of sophisticated Technology CAD (TCAD) tools. These tools are well developed and based primarily upon semi-classical models, often augmented by some quantum mechanical corrections. Due to the aggressive scaling of integrated transistors, however, quantum mechanical effects become more and more important, rendering the applicability of these simulation methods questionable. One challenge in TCAD that can be clearly identified is the development of new simulation methods adequately describing carrier transport in nano-electronic

devices. Today this field of research is addressed by many research groups. The formulations of quantum transport used are based on the density matrix, non-equilibrium Green's functions, the Wigner function, and the Pauli Master equation. The simpler case of quantum-ballistic transport is covered by the Schrödinger equation supplemented by open boundary conditions.

On the other hand, semi-classical transport in semiconductor devices is well understood, especially through the availability of Monte Carlo simulation tools which provide an accurate solution to the Boltzmann equation. Elaborate models of band-structure and scattering mechanisms can be included. Fig. 1 shows the interrelation between the three groups of transport models. In this taxonomy quantum transport is assumed to be time irreversible, whereas quantum ballistic transport uses a time reversible description. If scattering, which is often described in a time irreversible manner by the Fermi Golden Rule approximation, is neglected in the von Neumann equation or the Dyson equation, these formulations simplify to quantum ballistic ones, as indicated by the arrows in Fig. 1. In the semi-classical limit the Wigner equation simplifies to the Boltzmann equation. Irreversibility of the latter has already been proven by Boltzmann by means of the H-theorem.

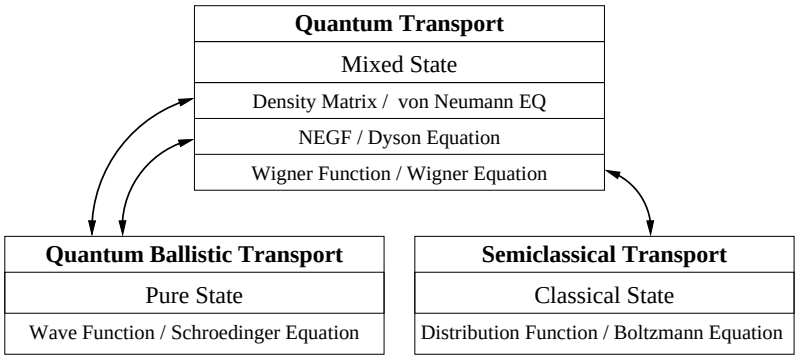

Fig. 1. Hierarchy of transport equations in semiconductor current transport modeling.

A semiconductor device often represents a multi-scale problem, where quantum mechanical effects occur in some small active region embedded in an extended classical region. Such situations call for the introduction of hybrid approaches, connecting semi-classical and quantum transport models.

All transport models, independently of their complexity, need to be coupled to the Poisson equation

$$\nabla \cdot (\kappa \nabla \varphi) = -\rho(\varphi)\,, \qquad \rho(\varphi) = \mathrm{q}(p - n + C) \tag{1}$$

which determines the self-consistent electrostatic potential φ. The transport model gives an in general non-linear dependence of the space charge density ρ on the potential φ. Of utmost importance from a numerical point of view is the availability

of efficient and robust iteration schemes for the solution of the non-linear system of model equations.

Section 2 addresses demands on semi-classical transport models, including moment equations, the Monte Carlo method, applications to strained semiconductors, and quantum-corrections. Extensions of semi-classical models by quantum corrections and tunneling models are the subject of Section 3. Section 4 deals with different formulations of quantum-ballistic transport such as tunneling models, adiabatic decomposition and the quantum transmitting boundary method. As typical applications multi-gate SOI FETs and carbon nanotube FETs are presented. Finally, quantum transport in the Wigner function formulation is considered in Section 5. Applications to ultra-short double gate FETs and resonant tunneling diodes are discussed.

2. Semi-classical Transport

Although semi-classical transport in semiconductors is well understood, research on this subject is still needed for several reasons. Transport models based on the moments of the Boltzmann equation, such as drift-diffusion and energy transport, are well accepted in TCAD. With down-scaling, however, these transport descriptions are gradually losing validity. For TCAD applications the Monte Carlo method still does not represent an alternative due to excessive computation time requirements. An extension of the computationally more efficient moment-based transport models is therefore desirable. Demands on semi-classical transport calculations also arise from new effects currently exploited or investigated to increase transistor on-current. Such effects are for instance mobility enhancement in strained silicon and germanium channels, possibly in combination with a favorable substrate orientation and channel orientation. Detrimental effects due to new materials and new structures need to be quantified, such as mobility reduction in ultra-thin semiconductor films, remote Coulomb scattering or soft-phonon scattering in the presence of high-k materials.

The semi-classical description of charge transport in semiconductor devices is given by the Boltzmann equation [3].

$$\frac{\partial f}{\partial t} + \mathbf{u} \cdot \nabla_r f + \frac{s_\nu \, \mathrm{q}}{\hbar} \, \mathbf{E} \cdot \nabla_{\mathbf{k}} f = \left(\frac{\partial f}{\partial t} \right)_{\mathrm{coll}} \tag{2}$$

Here, $f(\mathbf{r}, \mathbf{k}, t)$ is the distribution function of carriers in phase space, formed by position $\mathbf{r}$ and momentum ($\hbar\mathbf{k}$). The charge sign s_ν distinguishes between electrons and holes, $\nu = n, p$. The right-hand side represents the collision operator which describes scattering of particles due to phonons, impurities, interfaces, and various other scattering sources. However, for realistic structures, a direct numerical solution of this equation by discretization of the phase space is computationally prohibitive. Approximate solutions can be obtained by the method of moments. Monte Carlo methods allow accurate evaluation of the moments of f.

2.1. *Moment Equations*

Most widely used in TCAD are the drift-diffusion model, based on two moments of the Boltzmann equation, and the energy transport model, based on four moments. Currently six moments transport models are being developed [4]. Such models, while computationally still efficient compared to the Monte Carlo method, provide additional information on the shape of the distribution function, which allows construction of improved models for hot-carrier effects, such as avalanche generation, hot-carrier induced gate currents, hot-carrier diffusion in an SOI floating body, and non-local effects in the deca-nanometer regime.

Using the method of moments one constructs equations for statistical averages defined as

$$\langle \Phi \rangle = \frac{1}{4\pi^3} \int \Phi(\mathbf{k})\, f(\mathbf{r}, \mathbf{k}, t)\, \mathrm{d}^3 k\,, \tag{3}$$

where $\Phi(\mathbf{k})$ is a freely chosen weight function. Each term of (2) is multiplied by a set of suitable weight functions and integrated over $\mathbf{k}$-space. This yields a set of time-dependent differential equations in $\mathbf{r}$-space. This procedure generates an infinite set of equations which must be closed by a suitably chosen ansatz. The weight functions are scalars for even orders and vectors for odd orders. Commonly the following physically-motivated weight functions are chosen.

$$\begin{aligned} &\Phi_0 = 1 && \Phi_2 = \mathcal{E} && \Phi_4 = \mathcal{E}^2 \\ &\Phi_1 = \hbar\,\mathbf{k} && \Phi_3 = \mathbf{u}\,\mathcal{E} && \Phi_5 = \mathbf{u}\,\mathcal{E}^2 \end{aligned} \tag{4}$$

Taking the moment of the Boltzmann equation gives the following general moment equation,

$$\frac{\partial \langle \Phi_j \rangle}{\partial t} + \nabla_{\mathbf{r}} \cdot \langle \mathbf{u} \otimes \Phi_j \rangle - s_\nu\, \mathrm{q}\, \mathbf{E} \cdot \langle \nabla_{\mathbf{p}} \otimes \Phi_j \rangle = \int \mathrm{d}^3\, k\, \Phi_j \left(\frac{\partial f}{\partial t} \right)_{\mathrm{coll}} \tag{5}$$

where $\otimes$ denotes the tensor product. To obtain a closed set of equations several approximations have to be made. One concerns the moment of the scattering integral, which is frequently approximated by a macroscopic relaxation time expression of the form

$$\int \mathrm{d}^3 k \Phi_j \left(\frac{\partial f}{\partial t} \right)_{\mathrm{coll}} \cong -\frac{\langle \Phi \rangle - \langle \Phi \rangle_0}{\tau_\Phi} \tag{6}$$

The distribution function can be split in its symmetric and antisymmetric part. In the diffusion approximation it is assumed that the antisymmetric part is small compared to the symmetric part, which implies that the displacement of the distribution function is small compared to its width. As a consequence, the symmetric part will be isotropic, thus depending only on the modulus of $\mathbf{k}$.

$$f(\mathbf{k}) = f_S(|\mathbf{k}|) + f_A(\mathbf{k}) \tag{7}$$

With this assumption all tensor-valued averages become scalar quantities. Finally, it can be argued that at technical frequencies the time derivatives of the fluxes can be neglected. As a result one obtains the following balance equations

$$\frac{\partial\langle 1\rangle}{\partial t} + \nabla\cdot\langle\mathbf{u}\rangle = 0 \tag{8}$$

$$\frac{\partial\langle\mathcal{E}\rangle}{\partial t} + \nabla\cdot\langle\mathbf{u}\,\mathcal{E}\rangle - s_\nu\,\mathrm{q}\,\mathbf{E}\cdot\langle\mathbf{u}\rangle = -\frac{\langle\mathcal{E}\rangle-\langle\mathcal{E}\rangle_0}{\tau_\mathcal{E}} \tag{9}$$

$$\frac{\partial\langle\mathcal{E}^2\rangle}{\partial t} + \nabla\cdot\langle\mathbf{u}\,\mathcal{E}^2\rangle - s_\nu\,2\,\mathrm{q}\,\mathbf{E}\cdot\langle\mathbf{u}\,\mathcal{E}\rangle = -\frac{\langle\mathcal{E}^2\rangle-\langle\mathcal{E}^2\rangle_0}{\tau_\Theta} \tag{10}$$

and the following flux equations

$$\frac{2}{3}\,\nabla\langle\mathcal{E}\rangle - s_\nu\,\mathrm{q}\,\mathbf{E}\,\langle 1\rangle = -m_\nu\,\frac{\langle\mathbf{u}\rangle}{\tau_m} \tag{11}$$

$$\frac{2}{3}\,\nabla\langle\mathcal{E}^2\rangle - s_\nu\,\frac{5}{3}\,\mathrm{q}\,\mathbf{E}\,\langle\mathcal{E}\rangle = -m_\nu\,\frac{\langle\mathbf{u}\,\mathcal{E}\rangle}{\tau_S} \tag{12}$$

$$\frac{2}{3}\,\nabla\langle\mathcal{E}^3\rangle - s_\nu\,\frac{7}{3}\,\mathrm{q}\,\mathbf{E}\,\langle\mathcal{E}^2\rangle = -m_\nu\,\frac{\langle\mathbf{u}\,\mathcal{E}^2\rangle}{\tau_K} \tag{13}$$

In analogy to the energy-transport model new variables are introduced, where ν denotes the carrier concentration, T_ν the carrier temperature, $\mathbf{J}_\nu$ the electrical current density, and $\mathbf{S}_\nu$ the energy flux density.

$$\langle 1\rangle = \nu, \qquad \langle\mathcal{E}\rangle = \frac{3}{2}\,\mathrm{k_B}\,\nu\,T_\nu, \qquad \langle\mathcal{E}^2\rangle = \frac{15}{4}\,\mathrm{k_B^2}\,\nu\,T_\nu\,\Theta_\nu, \qquad \langle\mathcal{E}^3\rangle = \frac{105}{8}\,\mathrm{k_B^3}\,\nu\,M_6$$

$$\langle\mathbf{u}\rangle = \frac{\mathbf{J}_\nu}{s_\nu\,\mathrm{q}}, \qquad \langle\mathbf{u}\,\mathcal{E}\rangle = \mathbf{S}_\nu, \qquad \langle\mathbf{u}\,\mathcal{E}^2\rangle = \mathbf{K}_\nu$$

The new variables are a second order temperature Θ_ν, the moment of sixth order M_6, and a flux $\mathbf{K}_\nu$ related to the kurtosis of the distribution function. Adding generation-recombination terms the balance equations become

$$\nabla\cdot\mathbf{J}_\nu = -s_\nu\,\mathrm{q}\,(\frac{\partial\nu}{\partial t} + R_\nu) \tag{14}$$

$$\nabla\cdot\mathbf{S}_\nu = -C_4\,\frac{\partial(\nu\,T_\nu)}{\partial t} + \mathbf{E}\cdot\mathbf{J}_\nu - C_4\,\nu\,\frac{T_\nu-T_L}{\tau_\mathcal{E}} + G_{\mathcal{E}_\nu} \tag{15}$$

$$\nabla\cdot\mathbf{K}_\nu = -C_5\,\frac{\partial(\nu\,T_\nu\,\Theta_\nu)}{\partial t} + 2\,s_\nu\,\mathrm{q}\,\mathbf{E}\cdot\mathbf{S}_\nu - C_5\,\nu\,\frac{T_\nu\,\Theta_\nu - T_L^2}{\tau_\Theta} + G_{\Theta_\nu} \tag{16}$$

$$C_4 = \frac{3}{2}\,\mathrm{k_B} \qquad C_5 = \frac{15}{4}\,\mathrm{k_B^2} \tag{17}$$

In the following flux equations the mobility $\mu_\nu = \mathrm{q}\tau_m/m_\nu$ is introduced:

$$\mathbf{J}_\nu = -C_1\left(\nabla(\nu\,T_\nu) - s_\nu\,\frac{\mathrm{q}}{\mathrm{k_B}}\,\mathbf{E}\,\nu\right) \qquad C_1 = s_\nu\,\mathrm{k_B}\,\mu_\nu \tag{18}$$

$$\mathbf{S}_\nu = -C_2\left(\nabla(\nu\,T_\nu\,\Theta_\nu) - s_\nu\,\frac{\mathrm{q}}{\mathrm{k_B}}\,\mathbf{E}\,\nu\,T_\nu\right) \qquad C_2 = \frac{5}{2}\,\frac{\mathrm{k_B^2}}{\mathrm{q}}\,\frac{\tau_S}{\tau_m}\,\mu_\nu \tag{19}$$

$$\mathbf{K}_\nu = -C_3\left(\nabla(\nu\,M_6) - s_\nu\,\frac{\mathrm{q}}{\mathrm{k_B}}\,\mathbf{E}\,\nu\,T_\nu\,\Theta_\nu\right) \qquad C_3 = \frac{35}{4}\,\frac{\mathrm{k_B^3}}{\mathrm{q}}\,\frac{\tau_K}{\tau_m}\,\mu_\nu \tag{20}$$

The drift-diffusion transport model consists of the continuity equation (14) and the current relation (18). The latter is decoupled from the next higher equation by introducing a closure assumption on the second order moment, $T_\nu = T_L$. The physical meaning is that the carrier gas is in equilibrium with the lattice. From an engineering point of view, the drift-diffusion model has proven amazingly successful due to its efficiency and numerical robustness. These properties make feasible two- and three-dimensional numerical studies on fairly large unstructured grids. The robustness comes from the fact that in this approach the current density is given by a potential flow with the gradient of the quasi-Fermi level as the driving force. However, several shortcomings of this model are critical for miniaturized devices. Especially hot-carrier effects such as impact ionization may be difficult to estimate and non-local effects such as velocity overshoot are neglected entirely.

Higher-order transport models such as the hydrodynamic [5] and energy-transport [6] models are supposed to overcome some of the shortcomings of the drift-diffusion model. The energy-transport model takes into account additionally the carrier energy balance equation (15) and the energy flux equation (19). An assumption on the fourth order moment has to be made to close the system. Assuming a heated Maxwellian distribution for the symmetric part gives the closure relation $\Theta_\nu = T_\nu$. Implementations of the energy-transport model are available in commercial and academic device simulators. However, problems with the energy-transport model for TCAD applications are manyfold. It typically tends to overestimate non-local effects and thus the on-current of a device. With the heated Maxwellian assumption implicit in the model the high energy tail of the carrier distribution is often considerably overestimated. This may result in unacceptable errors, for example, in the estimation of the hot carrier induced gate tunneling current [7]. For the specific situation of a partially-depleted SOI MOSFET it has been shown that the energy-transport model may fail completely in predicting the device characteristics. The reason is an overestimation of hot carrier diffusion into the floating body of the device [8].

Going one step further in the model hierarchy results in a transport model of sixth order. A balance equation for the average squared energy (16) and the related flux equation (20) are added. To close the equation system, the moment of sixth order M_6 has to be approximated using the lower order moments. For a Maxwellian distribution function and parabolic bands one would obtain $M_6 = T_\nu^3$. However, as the six-moments model goes beyond the heated-Maxwellian approximation by treating the kurtosis of the distribution function as an unknown a more general closure relation is desirable. In [9] an empirical closure relation has been proposed taking into account also the second order Temperature Θ_ν.

$$M_6 = T_\nu^3 \left(\frac{\Theta_\nu}{T_\nu}\right)^c \tag{21}$$

From Monte Carlo simulations, which are considered to be an accurate reference, the ratio M_6^{MC}/M_6 has been analyzed to determine the free parameter c in (21).

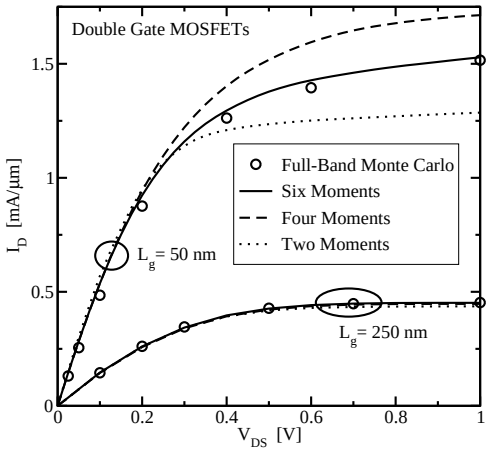

Fig. 2. Comparison of macroscopic transport models with full-band Monte Carlo. While all models yield similar results at large gate lengths, only the six-moments model reproduces the short-channel Monte Carlo results.

In [10] a value of $c = 2.7$ has been estimated. Compared to the energy-transport models, two additional relaxation times are needed, namely the relaxation time of the second order temperature τ_Θ, and the kurtosis flux relaxation time τ_K. Since analytical models for these new parameters are not available, in [10] tabulated parameter values obtained from bulk Monte Carlo simulations are used.

Sonoda *et al.* [11] proposed a similar six moments transport model, however, with a very restrictive closure relation. Another difference is that they used a microscopic relaxation time approximation as proposed by Stratton [6], whereas in the equations above the macroscopic relaxation time approximation (6) is employed.

As a calibration tool, the full-band Monte Carlo method has become accepted, since it can precisely account for the various scattering processes in the scattering operator [12]. Fig. 2 shows a comparison of different macroscopic simulation approaches with full-band Monte Carlo results for a 250 nm and a 50 nm double-gate MOSFET [10]. It can be seen that transport models based on two, four, and six moments deliver similar results for the long-channel device, while only the six moments model is able to reproduce the full-band Monte Carlo results for the short-channel device.

2.2. *The Monte Carlo Method*

The Monte Carlo method is well established for studying semiconductor devices and exploring semiconductor properties. The method simulates the motion of charge carriers in the six-dimensional phase space formed by position and momentum. Subjected to the action of an external force field, the point-like carriers follow tra-

jectories governed by Newton's law and the carrier's dispersion relation. These drift processes are interrupted by scattering events which are assumed local in space and instantaneous in time. The duration of a drift process, the type of scattering mechanism, and the state after scattering are selected randomly from given probability distributions characteristic to the microscopic process. The method of generating sequences of drift processes and scattering events appears so transparent from a physical point of view, that it is frequently interpreted as a direct emulation of the physical process rather than as a numerical method. In fact, the Monte Carlo algorithms employed in device simulation were originally devised from merely physical considerations, viewing a Monte Carlo simulation as a simulated experiment. These algorithms are Ensemble Monte Carlo [13][14] and One Particle Monte Carlo [15][16]. The alternative way, namely to state the transport equation first and to formulate then a Monte Carlo algorithm for its solution, has been reported end of the 1980's [17] [18]. A link between physically-based Monte Carlo methods and numerical Monte Carlo methods for solving integrals and series of integrals has been established [19].

In [17] the Boltzmann equation is transformed to an integral equation which is then iteratively substituted into itself. The resulting iteration series is evaluated by a new Monte Carlo technique, called *Monte Carlo Backward* (MCB) since the trajectories are followed back in time. All trajectories start from the chosen phase space point, and their number is freely adjustable and not controlled by the physical process. MCB allows for the evaluation of the distribution function in a given point with a desired precision. The algorithm is useful if rare events have to be simulated or the distribution function is needed only in a small phase space domain. Since the original MCB algorithm turned out to be instable, a stable variant has been proposed in [20].

The *weighted ensemble Monte Carlo* (WEMC) method allows the use of arbitrary probabilities for trajectory construction, such that particles can be guided to a phase space region of interest [21][22]. The unbiased estimator for the distribution function contains a product of weights which are given by the ratio of the real and the modified probabilities of the selected events.

The large variations of the carrier concentration in a realistic device impose severe problems upon the common MC algorithms. Statistical enhancement methods are required to reduce the variance in rarely visited phase space regions of interest. Trajectory multiplication schemes used in various MC device simulators [23][24][25] are extensions of the method of Phillips and Price [26]. Several variable-weight or population control techniques have been developed for the EMC [27][28][29][30]. A comparison of statistical enhancement methods is given in [31]. Application of the event bias technique to variance reduction in device simulation is reported in [32][33]. The MCB method is another powerful technique to simulate rare events, whose potential is yet to be employed in future applications.

The work of Kurosawa in 1966 [34] is considered to be the first account of an application of the MC method to high-field transport in semiconductors. The fol-

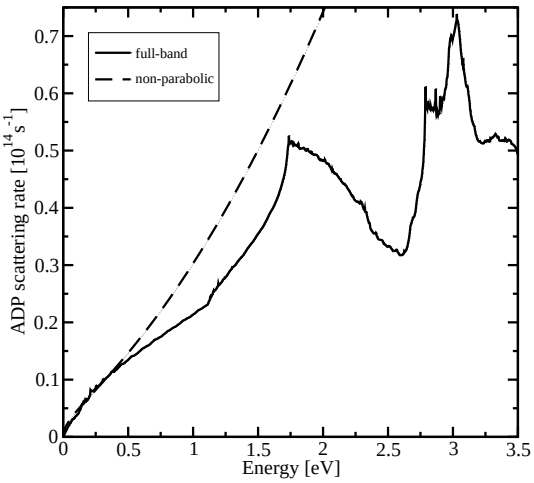

Fig. 3. Acoustic deformation potential scattering rate of electrons in silicon for analytical and numerical band structure models.

lowing decade has seen considerable improvement of the method and application to a variety of materials [35]. Early papers deal with gallium arsenide [36] and germanium [37]. In the mid 1970s a physical model of silicon has been developed, capable of explaining major macroscopic transport characteristics [38][39]. The used band structure models were represented by simple analytic expressions accounting for non-parabolicity and anisotropicity. With the increase of the energy range of interest then the need for accurate, numerical band structure models arose [40][12] [41][42]. For electrons in silicon, the most thoroughly investigated case, it is believed that a satisfactory understanding of the basic scattering mechanisms at high energies has been reached, giving rise to a new "standard model" [43]. The effect of the band structure model on the scattering rate is shown in Fig. 3. Of paramount practical relevance are the transport properties of carriers in FET channels. A large normal field in a bulk device or the geometric confinement in a thin semiconductor film give rise to size quantization and the formation of subbands. Especially with the introduction of strain in the channel region research on classical transport in a subband system has regained considerable interest [44,45]. The effect of size quantization on the scattering rate is shown in Fig. 4.

2.3. *Strain Effects*

In the last years enormous research efforts have been devoted to the study of new materials compatible with silicon technology and new device structures for improving the speed of ULSI circuits. Strained silicon has emerged as a promising material, since it offers both higher electron and hole mobility than unstrained silicon. In some cases improvement by a factor of more than two was both theoret-

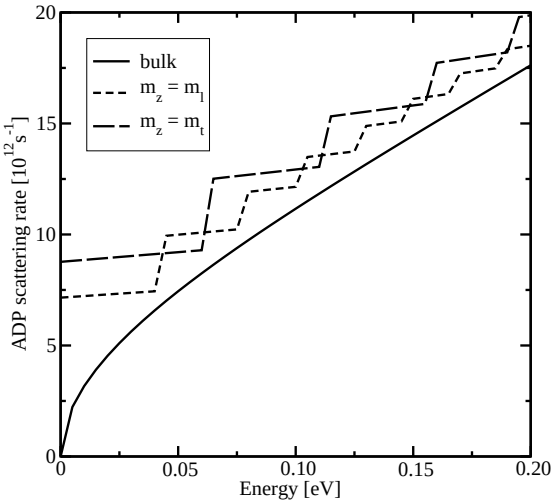

Fig. 4. Acoustic deformation potential scattering rate of electrons in a silicon inversion layer. Due to the anisotropic effective mass two subband ladders are formed.

ically predicted and experimentally confirmed. Strained silicon layers are achieved by epitaxial growth on SiGe buffers. Due to the lattice mismatch, a pseudomorphically grown silicon layer on a relaxed SiGe buffer experiences a biaxial tensile strain, provided that the layer thickness is below a critical value to prevent strain relaxation. Both compressively and tensile, uniaxially strained silicon channels have been achieved by specific process variants [46]. Biaxial strain leads to a modification of the conduction band, as shown in Fig. 5. The 6-fold degenerate Δ_6-valleys in silicon is being split into 2-fold degenerate Δ_2 valleys (lower in energy) and 4-fold degenerate Δ_4 valleys (higher in energy). The lower in-plane effective mass of electrons in the Δ_2 valleys and the reduction of inter-valley phonon scattering lead to an enhancement of electron mobility. To enable predictive TCAD simulations a reliable set of models for the Si/SiGe material system is required. Such a set has to include models for the band structure parameters and deformation potentials. Pseudopotential calculations have been reported in [47,48]. The transport properties of strained silicon or SiGe layers have been theoretically investigated using Monte Carlo calculations [49,50,51,52,53] or near equilibrium solutions to the Boltzmann equation [47]. A comprehensive set of strain-dependent models for parameters such as the low-field, high-field and the surface mobility, energy relaxation time and carrier life times for Technology CAD purposes is yet to be developed. Possible approaches are to further use analytical models or tabulated Monte Carlo data in a device simulator [54].

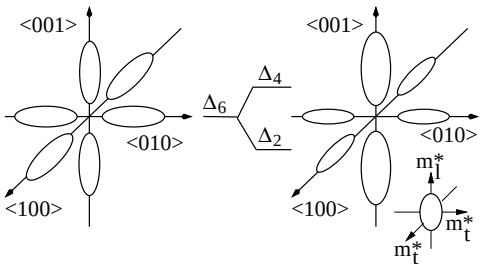

Fig. 5. Conduction band splitting in tensile-strained silicon (right) compared to unstrained silicon (left).

3. Quantum Effects

Within the macroscopic transport models presented above, quantum-mechanical effects are usually accounted for by means of quantum corrections in the continuity equations. However, the fabrication of structures in the nanometer regime triggered the development of quantum-mechanical modeling tools. Such tools became especially important for the evaluation of gate dielectrics, which represent the smallest feature scale in microelectronics. Neglecting quantum confinement in this regime leads to results which are not just slightly inaccurate, but systematically wrong. As an example, the CV-characteristics of an 1.5 nm dielectric layer is shown in Fig. 6 for different poly doping concentrations calculated classically and quantum-mechanically and showing a large discrepancy under inversion conditions. This apparent inaccuracy of conventional models justified the development of one-dimensional quantum device simulators which are today established tools for the characterization of gate dielectric layers [55,56,57]. One-dimensional solutions of the Schrödinger equation are also frequently used to derive correction factors for the carrier concentration calculated by macroscopic transport models [58,59,60]. They can be used to yield a quick estimate of quantum-confinement related effects without degrading the efficiency of the device simulator used. However, based on the closed-boundary Schrödinger equation charge transport is neglected.

A quantum correction to classical Monte Carlo simulations has been attempted by using an effective potential instead of the self-consistent potential determined by the Poisson equation [61,62]. The effective potential can be obtained by a convolution of the electrostatic potential with a Gaussian function which leads to a smoothing of the original potential. A quantum correction based on the Schrödinger equation applied to a full-band Monte Carlo simulator is reported in [63].

4. Quantum-Ballistic Transport

The term quantum-ballistic designates quantum-mechanical current transport without energy dissipating scattering processes. Quantum-ballistic models are often applied to the simulation of gate leakage caused by tunneling.

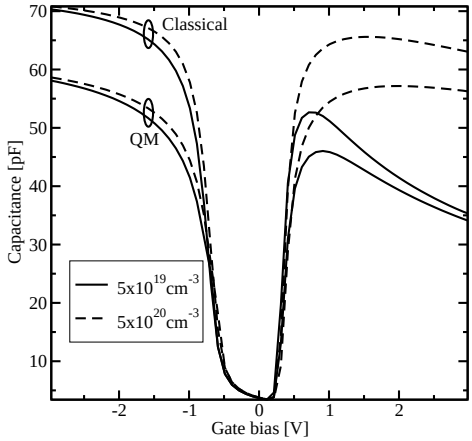

Fig. 6. Comparison of CV characteristics of a 1.5 nm dielectric layer with different polysilicon doping applying one-dimensional classical and quantum-mechanical simulations.

4.1. *Tunneling Models*

The central quantity for the description of tunneling is the transmission coefficient $TC(\mathcal{E})$. It is used in the so-called Tsu-Esaki formula [64] to determine the tunneling current density.

$$J = \frac{4\pi m_{\mathrm{eff}} \mathrm{q}}{h^3} \int_{\mathcal{E}_{\min}}^{\mathcal{E}_{\max}} TC(\mathcal{E}_x) N(\mathcal{E}_x)\, \mathrm{d}\mathcal{E}_x \tag{22}$$

The supply function $N(\mathcal{E}_x)$ depends on the carrier distribution function at the interface. Various methods such as the Wentzel-Kramers-Brillouin (WKB), the transfer-matrix, and quantum transmitting boundary method have been proposed to calculate the transmission coefficient [65]. The resulting tunneling currents can be incorporated into moment-based transport models by adding generation/recombination terms to the continuity equation.

4.2. *Adiabatic Decomposition*

The ongoing reduction of channel lengths raises the need for a fully quantum-mechanical treatment of carrier transport. This makes the solution of Schrödinger's equation with open boundary conditions necessary, which can be accomplished by means of the quantum transmitting boundary method as shown in [66,67]. An established and sophisticated framework for these calculations is based on the non-equilibrium Green's Function method, which has been used for one-dimensional studies of resonant tunneling diodes [68]. Two- and three-dimensional quantum

ballistic simulations can be performed by means of an adiabatic decomposition of wave functions into one or two confinement directions [69,70].

The idea of adiabatic decomposition is demonstrated in the following for a two-dimensional structure with potential $V(x,z)$ [71]. Here it is assumed that z denotes the direction normal to a channel and that current is predominantly flowing in x direction. The starting point is the two-dimensional Schrödinger equation.

$$-\frac{\hbar^2}{2}\left(\frac{1}{m_x}\frac{\partial^2}{\partial x^2}+\frac{1}{m_z}\frac{\partial^2}{\partial z^2}\right)\psi(x,z)+V(x,z)\psi(x,z)=E\psi(x,z) \tag{23}$$

With respect to the z-coordinate the wave function $\psi(x,z)$ is now expanded in a series.

$$\psi(x,z)=\sum_n \phi_n(x)\,\zeta_n(z;x) \tag{24}$$

The basis ζ_n is obtained from a solution of the one-dimensional Schrödinger equation in transverse direction at some given lateral position x_0.

$$-\frac{\hbar^2}{2m_z}\frac{\partial^2}{\partial z^2}\zeta_n(z;x_0)+V(x_0,z)\zeta_n(z;x_0)=\epsilon_n(x_0)\zeta_n(z;x_0) \tag{25}$$

The eigenvalue $\epsilon_n(x)$ gives the position-dependent energy of the n-th subband. The expansion coefficients $\phi_n(x)$ are determined by a coupled system of Schrödinger equations with coupling coefficients A_{nm} and B_{nm}.

$$\begin{aligned}-\frac{\hbar^2}{2m_x}\frac{\mathrm{d}^2}{\mathrm{d}x^2}\phi_n(x)+\big(\epsilon_n(x)+A_{nn}(x)\big)\phi_n(x)\\ +\sum_{m\neq n}\left(A_{nm}(x)\phi_m(x)+B_{nm}(x)\frac{\mathrm{d}\phi_m}{\mathrm{d}x}\right)=E_n\phi_n(x)\end{aligned} \tag{26}$$

$$A_{nm}(x)=-\frac{\hbar^2}{2m_z}\int \zeta_n(z;x)\frac{\partial^2\zeta_m(z;x)}{\partial z^2}\,\mathrm{d}z \tag{27}$$

$$B_{nm}(x)=-\frac{\hbar^2}{m_z}\int \zeta_n(z;x)\frac{\partial\zeta_m(z;x)}{\partial z}\,\mathrm{d}z \tag{28}$$

In the adiabatic approximation the coupling terms are neglected. The problem simplifies to a solution of decoupled one-dimensional Schrödinger equations for each subband.

The adiabatic decomposition can typically be applied to the channel of a FET. Fig. 7 depicts a cross-section through the channel of different multi-gate silicon-on-insulator devices, namely a FinFET and a Π-gate FET [72]. Three-dimensional device simulations have been performed for turned-off devices (V_{DS}=1.0 V, V_{GS}=0.0 V) by means of coupling a two-dimensional Schrödinger-Poisson solver to the device simulator MINIMOS-NT [73], and the figures show the resulting carrier concentrations. While only the gate-all-around structure can fully deplete the channel, the Π-gate FET efficiently shields the channel from the drain bias, while posing only moderate additional process complexity [74].

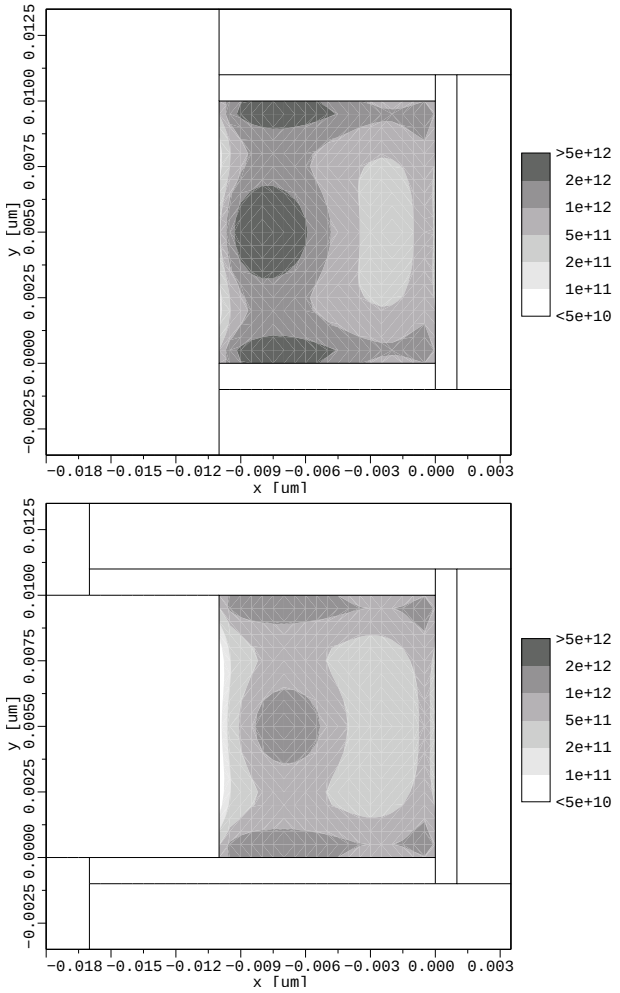

Fig. 7. Carrier concentration in the middle of the channel of a turned-off triple-gate FinFET (top) and a Π-FET (bottom). The Π-gate efficiently suppresses the spurious drain field.

Carbon nanotube (CNT) transistors can also be well described by one-dimensional effective Schrödinger equations resulting from an adiabatic decomposition. CNTs have emerged as promising candidates for nanoscale field effect transistors. High performance devices were achieved recently [75,76]. The contact between metal and CNT can be of Ohmic [77] or Schottky type [78,79,80]. Schottky contact CNTFETs operate by modulating the transmission coefficients of the Schottky barriers at the metal-CNT interfaces [80,81]. A CNTFET can be operated as an n-type or p-type device just by applying positive or negative voltages to the gate and drain contacts [82]. Two important figures of merit of FETs are the subthreshold slope and the $I_{\mathrm{on}}/I_{\mathrm{off}}$ ratio. To improve these parameters the coupling

between gate and CNT should be increased. This can be achieved by using thin high-κ materials as a gate dielectric [76]. Due to ambipolar behavior of Schottky barrier CNT-FETs the off-current is often intolerably high [82,83,84]. The reason of this behavior is that carrier injection at the source and drain contacts is controlled by the same gate, hence by increasing the coupling between the gate and the CNT the off-current also increases. To suppress the ambipolar behavior a double gate structure for CNTFETs has been proposed [85], see Fig. 8. Using this structure the carrier injection at the source and drain contacts can be separately controlled. For an n-type device electron injection at the source contact can be controlled by the first gate, while detrimental hole injection at the drain contact can be reduced by the second gate. Thus, the ambipolar behavior of CNTFETs can be completely suppressed, as seen in Fig. 9.

4.3. *Multi-dimensional Schrödinger Solvers*

Recently, simulators providing a fully two-dimensional solution of the open-boundary Schrödinger equation have been reported and applied to the simulation of 10 nm double-gate MOSFETs [86,87]. Besides the requirement for a fine and sometimes even equidistant mesh, a main obstacle in these approaches is that the treatment of scattering is not straightforwardly possible. Furthermore, these simulators are usually limited to specific geometries, restrictive grids, or small length scales, which makes their usability for engineering applications questionable. Nevertheless, these simulation approaches are necessary for the estimation of upper bounds of current transport at the quantum limit.

5. Quantum Transport

The methods described so far are either based on the assumption of pure classical or pure quantum transport. Modern microelectronic devices, however, are characterized by the transition between large reservoirs with strong carrier scattering, and

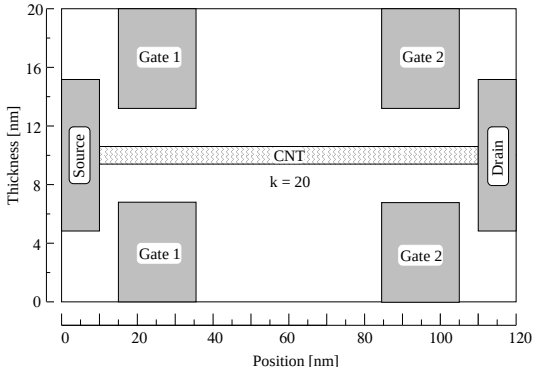

Fig. 8. Structure of a coaxial double gate carbon CNTFET.

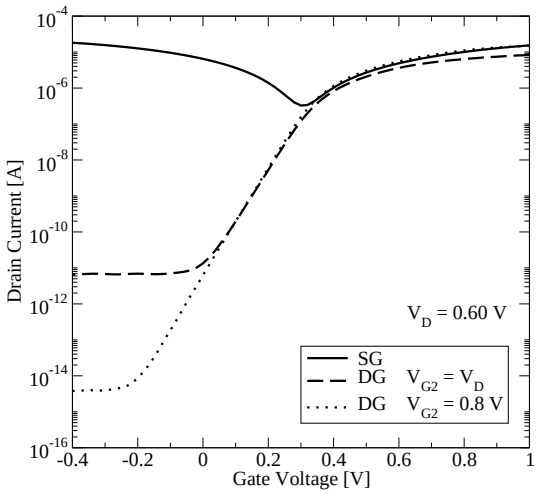

Fig. 9. Transfer characteristics of single gate (SG) and double gate (DG) CNT transistors with two different voltages on the second gate.

small regions where quantum effects are important or even dominate. To first order, quantum correction models can account for these effects. A more rigorous approach is to consider models derived from the Wigner equation. The Wigner function is given by a transformation of the density matrix [88,89].

$$f_{\mathrm{w}}(\mathbf{r},\mathbf{k},t) = \int \rho\left(\mathbf{r}+\frac{\mathbf{s}}{2},\mathbf{r}-\frac{\mathbf{s}}{2},t\right)\exp(-\imath\mathbf{k}\cdot\mathbf{s})\,\mathrm{d}\mathbf{s} \tag{29}$$

The kinetic equation for the Wigner function is similar to the Boltzmann equation, however with an additional potential operator at the right-hand side.

$$\left(\frac{\partial}{\partial t}+\mathbf{u}\cdot\nabla_r+\frac{s\,\mathrm{q}}{\hbar}\mathbf{E}\cdot\nabla_k\right)f_{\mathrm{w}} = \int V_{\mathrm{w}}(\mathbf{r},\mathbf{k}-\mathbf{k}')f_{\mathrm{w}}(\mathbf{k}',\mathbf{r},t)\mathrm{d}\mathbf{k}' + \left(\frac{\partial f_{\mathrm{w}}}{\partial t}\right)_{\mathrm{coll}} \tag{30}$$

Here it is assumed that the potential is decomposed into a smoothly varying, classical component and a rapidly varying, quantum-mechanical component, $V = V_{\mathrm{cl}} + V_{\mathrm{qm}}$. The classical force is then defined as $s\mathrm{q}\mathbf{E} = -\nabla V_{\mathrm{cl}}$. The kernel of the potential operator is given by the Wigner-Weyl transform of the quantum-mechanical component.

$$V_{\mathrm{w}}(\mathbf{r},\mathbf{k}) = \frac{1}{\imath\hbar\,(2\pi)^3}\int\left(V_{\mathrm{qm}}\left(\mathbf{r}+\frac{\mathbf{s}}{2}\right)-V_{\mathrm{qm}}\left(\mathbf{r}-\frac{\mathbf{s}}{2}\right)\right)\exp\left(-i\mathbf{k}\cdot\mathbf{s}\right)\,\mathrm{d}\mathbf{s} \tag{31}$$

Using the method of moments, from (30) once can derive quantum drift-diffusion and quantum hydrodynamic models [90]. These models are more suitable for the implementation in device simulators than a Schrödinger-Poisson solver which strongly depends on non-local quantities. However, it was reported that, while the carrier concentration in the inversion layer of a MOSFET can be modeled correctly, the density gradient method fails to reproduce tunneling currents [91].

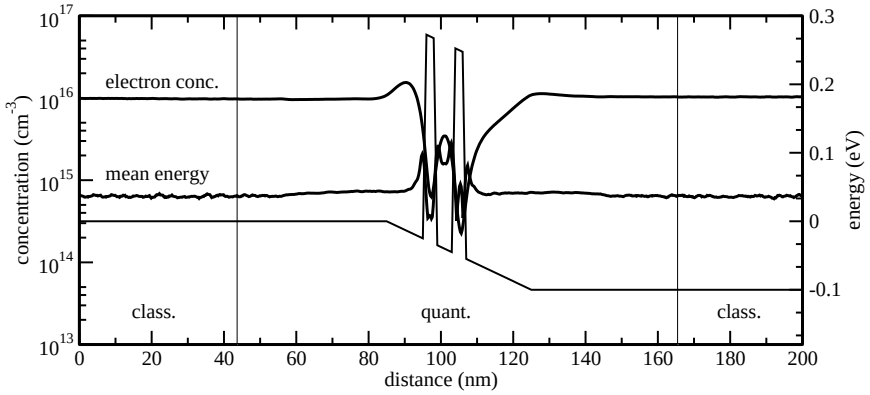

Fig. 10. Wigner Monte Carlo results of electron concentration and mean energy for a resonant tunneling diode.

Implementations of Monte Carlo methods for solving the Wigner device equation (30) have been reported [92,93]. Monte Carlo methods allow scattering processes to be included on a more detailed level [94,95], as compared to the finite-difference method [89] which is practically limited to a one-dimensional momentum space and the relaxation time approximation. Construction of new Monte Carlo algorithms is complicated by the fact that the kernel of the integral equation to solve is not positively defined. As a consequence, the commonly applied Markov Chain Monte Carlo method shows a variance exponentially increasing with time, prohibiting its application to realistic structures or larger evolution times [96,97,93]. Because of this so-called negative sign problem additional measures have to be introduced that prevent a run-away of the particle weights and hence of the variance [98,94].

This approach allows a unified treatment and a seamless transition between classical and quantum-mechanical regions in a device [98]. This method has been applied to the simulation of resonant tunneling diodes as shown in Fig. 10 and it was recently used for the simulation of 10 nm double-gate MOSFETs [99].

6. Conclusions

Semiconductor physics is a vast field and simulation approaches abound. Physicists are often tempted to use overly complicated approaches, in an understandable effort not to lose the important physics. However, some constraints for engineering application should be kept in mind. Models must be efficient: Timely results are often more valuable than accurate analyses [100]. There is a need for three-dimensional simulations, even if these are only rarely applied to check for spurious effects. Device simulators must allow a coupling with process simulators, since a detailed, physics-based transport model is of no use if geometry and doping are not described properly. Therefore, support of unstructured grids is necessary. Furthermore, the simulators should be for general-purpose and not limited to specific

geometries or simulation modes. It is still not clear which of the outlined quantum transport approaches will find its way into integrated TCAD environments, but its further success depends on efficient and accurate modeling of these new effects.

References

[1] "International technology roadmap for semiconductors – 2004 update," (2004), `http://public.itrs.net`.

[2] H. Iwai, "CMOS downsizing toward sub-10 nm," *Solid-State Electronics* **48**(4), 497 (2004).

[3] S. Selberherr, *Analysis and Simulation of Semiconductor Devices*, Springer Wien (1984).

[4] T. Grasser *et al.*, "Hot carrier effects within macroscopic transport models," *International Journal of High Speed Electronics and Systems* **13**(3), 873 (2003), (invited).

[5] K. Blotekjaer, "Transport equations for electrons in two-valley semiconductors," *IEEE Transactions on Electron Devices* **ED-17**(1), 38 (1970).

[6] R. Stratton, "Diffusion of hot and cold electrons in semiconductor barriers," *Physical Review* **126**(6) (1962).

[7] A. Gehring *et al.*, "Simulation of hot-electron oxide tunneling current based on a non-Maxwellian electron energy distribution function," *Journal of Applied Physics* **92**(10), 6019 (2002).

[8] M. Gritsch *et al.*, "Revision of the standard hydrodynamic transport model for SOI simulation," *IEEE Transactions on Electron Devices* **49**(10), 1814 (2002).

[9] T. Grasser *et al.*, "Using six moments of Boltzmann's transport equation for device simulation," *Journal of Applied Physics* **90**(5), 2389 (2001).

[10] T. Grasser *et al.*, "Advanced transport models for sub-micrometer devices," in *Proceedings International Conference on Simulation of Semiconductor Processes and Devices* (2004) 1–8.

[11] K. Sonoda *et al.*, "Moment expansion approach to calculate impact ionization rate in submicron silicon devices," *Journal of Applied Physics* **80**(9), 5444 (1996).

[12] M. Fischetti and S. Laux, "Monte Carlo analysis of electron transport in small semiconductor devices including band-structure and space-charge effects," *Physical Review B* **38**(14), 9721 (1988).

[13] R. Hockney and J. W. Eastwood, *Computer Simulation Using Particles*, Adam Hilger Bristol and Philadelphia (1988).

[14] C. Moglestue, "Monte Carlo particle modelling of small semiconductor devices," *Computer Methods in Applied Mechanics and Engineering* **30**, 173 (1982).

[15] P. J. Price, "Monte Carlo calculation of electron transport in solids," *Semiconductors and Semimetals* **14**, 249 (1979).

[16] C. Jacoboni and L. Reggiani, "The Monte Carlo method for the solution of charge transport in semiconductors with applications to covalent materials," *Reviews of Modern Physics* **55**(3), 645 (1983).

[17] C. Jacoboni *et al.*, "A new Monte Carlo technique for the solution of the Boltzmann transport equation," *Solid-State Electronics* **31**(3/4), 523 (1988).

[18] M. Nedjalkov and P. Vitanov, "Iteration approach for solving the Boltzmann equation with the Monte Carlo method," *Solid-State Electronics* **32**(10), 893 (1989).

[19] H. Kosina *et al.*, "Theory of the Monte Carlo method for semiconductor device simulation," *IEEE Transactions on Electron Devices* **47**(10), 1898 (2000).

[20] H. Kosina *et al.*, "A stable backward Monte Carlo method for the solution of the Boltzmann equation," in *Lecture Notes in Computer Science 2907: Large-Scale Scientific Computing* (2003) 170–177.

[21] C. Jacoboni, "A new approach to Monte Carlo simulation," in *International Electron Devices Meeting* (1989) 469–472.

[22] L. Rota *et al.*, "Weighted ensemble Monte Carlo," *Solid-State Electronics* **32**(12), 1417 (1989).

[23] E. Sangiorgi *et al.*, "MOS^2: An efficient Monte Carlo simulator for MOS devices," *IEEE Transactions on Computer-Aided Design of Integrated Circuits and Systems* **7**(2), 259 (1988).

[24] F. Venturi *et al.*, "A general purpose device simulator coupling Poisson and Monte Carlo transport with applications to deep submicron MOSFET's," *IEEE Transactions on Computer-Aided Design of Integrated Circuits and Systems* **8**(4), 360 (1989).

[25] H. Kosina and S. Selberherr, "A hybrid device simulator that combines Monte Carlo and drift-diffusion analysis," *IEEE Transactions on Computer-Aided Design of Integrated Circuits and Systems* **13**(2), 201 (1994).

[26] A. Phillips and P. Price, "Monte Carlo calculations on hot electron tails," *Applied Physics Letters* **30**(10), 528 (1977).

[27] T. Wang *et al.*, "Time-dependent ensemble Monte Carlo simulation for planar-doped GaAs structures," *Journal of Applied Physics* **58**(2), 857 (1985).

[28] S. Laux and M. Fischetti, "Numerical aspects and implementation of the DAMOCLES Monte Carlo device simulation program," in *Monte Carlo Device Simulation: Full Band and Beyond* 1–26. Kluwer Boston, Dordrecht, London (1991).

[29] M. Martín *et al.*, "Monte Carlo analysis of a Schottky diode with an automatic space-variable charge algorithm," *Semiconductor Science and Technology* **11**, 380 (1996).

[30] C. Jungemann *et al.*, "Phase space multiple refresh: A versatile statistical enhancement method for Monte Carlo device simulation," in *Proceedings International Conference on Simulation of Semiconductor Processes and Devices* (1996) 65–66.

[31] C. Wordelman *et al.*, "Comparison of statistical enhancement methods for Monte Carlo semiconductor simulation," *IEEE Transactions on Computer-Aided Design of Integrated Circuits and Systems* **17**(12), 1230 (1998).

[32] H. Kosina *et al.*, "An event bias technique for Monte Carlo device simulation," *Mathematics and Computers in Simulation* **62**(3-6), 367 (2003).

[33] M. Nedjalkov *et al.*, "The stationary Monte Carlo method for device simulation - part ii: Event biasing and variance estimation," *Journal of Applied Physics* **93**(6), 3564 (2003).

[34] T. Kurosawa, "Monte Carlo calculation of hot electron problems," in *Proceedings of the International Conference on the Physics of Semiconductors* (1966) 424–426.

[35] C. Jacoboni and P. Lugli, *The Monte Carlo Method for Semiconductor Device Simulation*, Springer Wien-New York (1989).

[36] W. Fawcett *et al.*, "Monte Carlo determination of electron transport properties in gallium arsenide," *Journal of Physics and Chemistry of Solids* **31**, 1963 (1970).

[37] W. Fawcett and E. Paige, "Negative differential mobility of electrons in germanium: A Monte Carlo calculation of the distribution function, drift velocity and carrier population in the $< 111 >$ and $< 100 >$ minima," *Journal of Physics C: Solid State Physics* **4**, 1801 (1971).

[38] C. Canali *et al.*, "Electron drift velocity in silicon," *Physical Review B* **12**(4), 2265 (1975).

[39] C. Jacoboni *et al.*, "Effects of band non-parabolicity on electron drift velocity in silicon above room temperature," *Journal of Physics and Chemistry of Solids* **36**, 1129 (1975).

[40] H. Shichijo and K. Hess, "Band-structure-dependent transport and impact ionization in GaAs," *Physical Review B* **23**(8), 4197 (1981).

[41] T. Kunikiyo *et al.*, "A Monte Carlo simulation of anisotropic electron transport in silicon including full band structure and anisotropic impact-ionization model," *Journal of Applied Physics* **75**(1), 297 (1994).

[42] P. Yoder *et al.*, "Monte Carlo simulation of hot electron transport in Si using a unified pseudopotential description of the crystal," *Semiconductor Science and Technology* **7**(3B), 357 (1992).

[43] M. Fischetti and S. Laux, "Monte Carlo simulation of electron transport in Si: The first 20 years," in *26th European Solid State Device Research Conference* (1996) 813–820.

[44] M. Fischetti *et al.*, "On the enhanced electron mobility in strained-silicon inversion layers," *Journal of Applied Physics* **92**(12), 7320 (2002).

[45] M. Fischetti and Z. Ren, "Six-band $k \cdot p$ calculation of the hole mobility in silicon inversion layers: Dependence on surface orientation, strain, and silicon thickness," *Journal of Applied Physics* **94**(2), 1079 (2003).

[46] S. E. Thompson *et al.*, "A logic nanotechnology featuring strained-silicon," *IEEE Electron Device Letters* **25**(4), 191 (2004).

[47] M. Fischetti and S. Laux, "Band structure, deformation potentials, and carrier mobility in strained Si, Ge, and SiGe alloys," *Journal of Applied Physics* **80**(4), 2234 (1996).

[48] M. Rieger and P. Vogl, "Electronic-band parameters in strained $Si_{1-x}Ge_x$ alloys on $Si_{1-y}Ge_y$ substrates," *Physical Review B* **48**(19), 14276 (1993).

[49] T. Vogelsang and K. Hofmann, "Electron transport in strained si layers on $Si_{1-x}Ge_x$ substrates," *Applied Physics Letters* **63**(2), 186 (1993).

[50] L. Kay and T.-W. Tang, "Monte Carlo calculation of strained and unstrained electron mobilities in $Si_{1-x}Ge_x$ using an improved ionized-impurity model," *Journal of Applied Physics* **70**(3), 1483 (1991).

[51] F. Bufler *et al.*, "Full band Monte Carlo investigation of electron transport in strained Si grown on $Si_{1-x}Ge_x$ substrates," *Applied Physics Letters* **70**, 2144 (1997).

[52] B. Fischer, *A Full-Band Monte Carlo Charge Transport Model for Nanoscale Silicon Devices Including Strain*, Shaker Verlag (2000).

[53] S. Smirnov and H. Kosina, "Monte Carlo modeling of the electron mobility in strained $Si_{1-x}Ge_x$ layers on arbitrarily oriented $Si_{1-y}Ge_y$ substrates," *Solid-State Electronics* **48**(9), 1325 (2004), (invited).

[54] F. Gamiz *et al.*, "Improving strained-Si on $Si_{1-x}Ge_x$ deep submicron MOSFETs performance by means of a stepped doping profile," *IEEE Transactions on Electron Devices* **48**(9), 1878 (2001).

[55] S. Jallepalli *et al.*, "Electron and hole quantization and their impact on deep submicron silicon p- and n-MOSFET characteristics," *IEEE Transactions on Electron Devices* **44**(2), 297 (1997).

[56] D. Vasileska *et al.*, "Scaled silicon MOSFET's: Degradation of the total gate capacitance," *IEEE Transactions on Electron Devices* **44**(4), 584 (1997).

[57] E. M. Vogel *et al.*, "A capacitance-voltage model for polysilicon-gated MOS devices including substrate quantization effects based on modification of the total semiconductor charge," *Solid-State Electronics* **47**, 1589 (2003).

[58] W. Hänsch *et al.*, "Carrier transport near the Si/SiO_2 interface of a MOSFET," *Solid-State Electronics* **32**(10), 839 (1989).
[59] M. vanDort *et al.*, "A simple model for quantisation effects in heavily-doped silicon MOSFETs at inversion conditions," *Solid-State Electronics* **37**(3), 411 (1994).
[60] C. Jungemann *et al.*, "Improved modified local density approximation for modeling of size quantization in NMOSFETs," in *Proceedings International Conference on Modeling and Simulation of Microsystems* (2001) 458–461.
[61] Y. Li *et al.*, "Modeling of quantum effects for ultrathin oxide MOS structures with an effective potential," *IEEE Transactions on Nanotechnology* **1**(4), 238 (2002).
[62] K. Z. Ahmed *et al.*, "On the evaluation of performance parameters of MOSFETs with alternative gate dielectrics," *IEEE Transactions on Electron Devices* **50**(12), 2564 (2003).
[63] B. Winstead and U. Ravaioli, "A quantum correction based on Schrödinger equation applied to Monte Carlo device simulation," *IEEE Transactions on Electron Devices* **50**(2), 440 (2003).
[64] R. Tsu and L. Esaki, "Tunneling in a finite superlattice," *Applied Physics Letters* **22**(11), 562 (1973).
[65] A. Gehring, *Simulation of Tunneling in Semiconductor Devices*, Dissertation, Technische Universität Wien (2003).
[66] C. S. Lent and D. J. Kirkner, "The quantum transmitting boundary method," *Journal of Applied Physics* **67**(10), 6353 (1990).
[67] W. Frensley, "Numerical evaluation of resonant states," *Superlattices and Microstructures* **11**(3), 347 (1992).
[68] R. Lake *et al.*, "Single and multiband modeling of quantum electron transport through layered semiconductor devices," *Journal of Applied Physics* **81**, 7845 (1997).
[69] F. O. Heinz *et al.*, "Full quantum simulation of silicon-on-insulator single-electron devices," *Journal of Computational Electronics* **1**(1), 161 (2002).
[70] G. Curatola *et al.*, "Modeling and simulation challenges for nanoscale MOSFETs in the ballistic limit," *Solid-State Electronics* **48**(4), 581 (2004).
[71] N. B. Abdallah *et al.*, "Simulation of 2D quantum transport in ultrashort DG-MOSFETS: A fast algorithm using subbands," in *Proceedings International Conference on Simulation of Semiconductor Processes and Devices* (2003) 267–270.
[72] J.-T. Park *et al.*, "Pi-gate SOI MOSFET," *IEEE Electron Device Letters* **22**(8), 405 (2001).
[73] Institut für Mikroelektronik Technische Universität Wien, Austria, *MINIMOS-NT 2.1 User's Guide* (2004).
[74] A. Gehring and S. Selberherr, "Evolution of current transport models for engineering applications," *Journal of Computational Electronics* (2005), in print.
[75] M. Radosavljevic *et al.*, "High performance of potassium n-doped carbon nanotube field-effect transistors," *Applied Physics Letters* **84**(18), 3693 (2004).
[76] B. M. Kim *et al.*, "High-performance carbon nanotube transistors on $SrTiO_3/Si$ substrates," *Applied Physics Letters* **84**(11), 1946 (2004).
[77] A. Javey *et al.*, "Ballistic carbon nanotube field-effect transistors," *Letters to Nature* **424**(6949), 654 (2003).
[78] R. Martel *et al.*, "Ambipolar electrical transport in semiconducting single-wall carbon nanotubes," *Physical Review Letters* **87**, 256805 (2001).
[79] J. Appenzeller *et al.*, "Field-modulated carrier transport in carbon nanotube transistors," *Physical Review Letters* **89**, 126801 (2002).
[80] S. Heinze *et al.*, "Carbon nanotubes as Schottky barrier transistors," *Physical Review Letters* **89**, 106801 (2002).

[81] J. Appenzeller *et al.*, "Tunneling versus thermionic emission in one-dimensional semiconductors," *Physical Review Letters* **92**, 048301 (2004).
[82] S. Heinze *et al.*, "Electrostatic engineering of nanotube transistors for improved performance," *Applied Physics Letters* **83**(24), 5038 (2003).
[83] M. Radosavljevic *et al.*, "Drain voltage scaling in carbon nanotube transistors," *Applied Physics Letters* **83**(12), 2435 (2003).
[84] J. Guo *et al.*, "A numerical study of scaling issues for Schottky barrier carbon nanotube transistors," *IEEE Transactions on Electron Devices* **51**(2), 172 (2004).
[85] M. Pourfath *et al.*, "Improving the ambipolar behavior of Schottky barrier carbon nanotube field effect transistors," in *Proc. ESSDERC* (2004) 429–432.
[86] S. Laux *et al.*, "Ballistic FET modeling using QDAME: Quantum device analysis by modal evaluation," *IEEE Transactions on Nanotechnology* **1**(4), 255 (2002).
[87] M. Sabathil *et al.*, "Towards fully quantum mechanical 3D device simulations," *Journal of Computational Electronics* **1**, 81 (2002).
[88] E. Wigner, "On the quantum correction for thermodynamic equilibrium," *Physical Review* **40**, 749 (1932).
[89] W. Frensley, "Boundary conditions for open quantum systems driven far from equilibrium," *Reviews of Modern Physics* **62**(3), 745 (1990).
[90] A. Wettstein *et al.*, "Quantum device-simulation with the density-gradient model on unstructured grids," *IEEE Transactions on Electron Devices* **48**(2), 279 (2001).
[91] T. Hoehr *et al.*, "On density-gradient modeling of tunneling through insulators," in *Proceedings International Conference on Simulation of Semiconductor Processes and Devices* (2002) 275–278.
[92] L. Shifren and D. Ferry, "Wigner function quantum Monte Carlo," *Physica B* **314**, 72 (2002).
[93] M. Nedjalkov *et al.*, "Wigner transport through tunneling structures - scattering interpretation of the potential operator," in *Proceedings International Conference on Simulation of Semiconductor Processes and Devices* (2002) 187–190.
[94] L. Shifren *et al.*, "Inclusion of nonlocal scattering in quantum transport," *Physics Letters A* **306**, 332 (2003).
[95] H. Kosina *et al.*, "Quantum Monte Carlo simulation of a resonant tunneling diode including phonon scattering," in *Nanotech* (2003) 190–193.
[96] F. Rossi *et al.*, "A Monte Carlo solution of the Wigner transport equation," *Semiconductor Science and Technology* **9**, 934 (1994).
[97] M. Nedjalkov *et al.*, "Convergency of the Monte Carlo algorithm for the Wigner quantum transport equation," *Journal of Mathematical and Computer Modelling* **23**(8/9), 159 (1996).
[98] H. Kosina *et al.*, "A Monte Carlo method seamlessly linking classical and quantum transport calculations," *Journal of Computational Electronics* **2**(2-4), 147 (2003).
[99] A. Gehring and H. Kosina, "Wigner-function based simulation of classic and ballistic transport in scaled DG-MOSFETs using the Monte Carlo method," *Journal of Computational Electronics* (2005), in print.
[100] M. Duane, "TCAD needs and applications from a users perspective," *IEICE Transactions on Electronics* **E82-C**(6), 976 (1999).